Intensity and temperature dependence of the steady-state light-induced defect density in *a*-Si:H

P. V. Santos, W. B. Jackson, and R. A. Street
Xerox Corporation, Palo Alto Research Center, 3333 Coyote Hill Rd., Palo Alto, California 94304
(Received 31 January 1991; revised manuscript received 10 June 1991)

The steady-state defect density in hydrogenated amorphous silicon (*a*-Si:H) under illumination was investigated for a wide range of illumination intensities and temperatures. The steady-state defect density under illumination is consistent with a chemical equilibrium model for defect generation, similar to the one used to describe defect generation in *a*-Si:H by doping and by thermal quenching. According to the model, defect generation is enhanced under illumination due to the reduction of the effective defect formation energy when the bands are populated by photogenerated carriers. Defect generation under illumination is a self-limiting process, and the defect density reaches a saturation value at long illumination time despite the existence of an extended distribution of defect formation sites.

I. INTRODUCTION

Hydrogenated amorphous silicon (*a*-Si:H) exhibits metastable defects caused by strong illumination,[1,2] doping,[3] carrier accumulation,[4] and rapid thermal quenching from high temperatures.[5] Metastable defect formation is one of the principal drawbacks for use of *a*-Si:H as the active layer in devices such as solar cells, light detectors, and thin-film transistors. Considerable effort has been devoted to understanding the origin and mechanisms of metastability. A major step in this direction has been the demonstration that defect formation is well described by a chemical equilibrium process involving hydrogen, defects, and a distribution of weak Si—Si bonds susceptible of being converted to defects.[6–8] Defect formation is then described by simple chemical reactions whose chemical equilibrium is shifted by external perturbation. The reaction kinetics is governed by dispersive hydrogen diffusion.

While the chemical equilibrium model satisfactorily describes defect creation by doping and quenching, it has not been successfully applied to light-induced defect generation. Recently, Park, Liu, and Wagner investigated the dependence of the density of light-induced defects in undoped *a*-Si:H on the illumination intensity.[9] They reported saturation values of $N_{s,\infty} \sim 10^{17}$ cm^{-3} for the density of light-induced defects at room temperature, independent of the illumination intensity. Since this value is below the defect density normally found in moderately doped material, this result has reopened the question of whether the saturation behavior is due to the depletion of precursor sites for defect generation, as would be expected if defects are associated with impurities,[10] or due to a steady-state balance between defect generation and annihilation, as required by the chemical equilibrium model.

In this paper, we investigated the saturation behavior of the density of light-induced defects in *a*-Si:H over a wide range of temperature and light intensities. The defect kinetics, which is more complicated and involves other assumptions, is dealt with in a separate paper.[11] The saturation density of light-induced defects is both temperature and light-intensity dependent, indicating that saturation is not caused by depletion of defect formation sites, as proposed in some models.[10] On the other hand, the light-intensity dependence of the saturation defect density is much weaker than that predicted by the model for light-induced defect formation proposed by Stutzmann, Jackson, and Tsai.[2] We will show here that the absolute values for the saturation density, and its temperature and light-intensity dependence, can be understood in the framework of a chemical equilibrium model similar to that used to describe defect creation by doping,[8] thermal quenching,[7] and carriers.[4] The model takes into account the existence of a distribution of weak bonds in the amorphous network and provides a connection between the Stabler-Wronski effect and chemical equilibration in *a*-Si:H.

II. EXPERIMENT

The samples used in this study are undoped *a*-Si:H grown by the glow discharge decomposition of pure silane. Most of the measurements were performed on 1.0-μm-thick samples grown at 230 °C on glass substrates, with a room-temperature defect density of 5×10^{15} cm^{-3}, determined by the constant photocurrent method (CPM). These measurements were performed in a coplanar configuration with contacts consisting of a 600-Å chromium layer over a 200-Å-thick 1 at. % phosphor-doped *a*-Si:H layer. The light-soaking experiments were performed with illumination intensities of 65, 700, and 2800 mW/cm^2. In the first two cases, the light source was a tungsten-halogen lamp with filter to cut wavelengths outside the range from 900 to 630 nm. For higher illumination intensities, the 6471-Å line of a Kr^+ laser was used. The electron-hole generation rates for the three intensities at 350 K are 1.5×10^{21}, 1.3×10^{22}, and 4×10^{22} cm^{-3} s^{-1}, respectively. Prior to each soaking experiment, the samples were annealed in dark at 500 K for at least 2 h and cooled down to the soaking temperature at a rate of $\sim$2 K/min.

The time dependence of the defect density during soaking was followed by a variation of the CPM method. The illumination was interrupted and the following steps were performed: (i) the ac photocurrent $I_{ph}(1.15\ eV)$ was measured for a low-intensity 1.15-eV illumination of photon flux $F(1.15\ eV)$, and (ii) the sample was then illuminated with 2-eV light and its photon flux $F(2\ eV)$ adjusted through a computer controlled feedback loop to obtain an ac photocurrent $I_{ph}(2\ eV)=I_{ph}(1.15\ eV)$. The energy of 1.15 eV was chosen because it lies sufficiently far away from the tail region so as to make the tail contribution negligible. The defect density was then taken to be proportional to the ratio $r_{CPM}=F(2\ eV)/F(1.15\ eV)$. This procedure allows the determination of the defect density in a relatively short time (30 to 40 s). It can be justified by the data shown in Fig. 1. Figure 1(a) shows CPM spectra in the annealed state at different temperatures. The spectra are normalized to the saturation value at 2.0 eV; at this energy the curves are approximately flat and decrease slowly to higher energies. For temperatures up to 350 K, there is no substantial change in the defect region (energies between 0.9 and 1.3 eV). The main difference in the spectra is a shift of the tail region to lower energies, consistent with a temperature variation of the band gap of ~ 0.4 meV/K. Above 400 K the CPM signal in the defect region increases with temperature, as we shall see in detail later. Figure 1(a) also includes the CPM spectra measured after light soaking at 350 K for a time long enough for the defect density to achieve its saturation value. The main effect of light soaking is to increase the absorption in the defect region by a constant (energy-independent) factor. This supports the use of the CPM signal at two single energies to evaluate light-induced changes in the defect density; absolute values for the defect density can be obtained by recording full CPM spectra before and after each soaking experiment, as shown in Fig. 1(a). Figure 1(b) compares the time evolution of the defect density N_s under illumination in a 15-μm-thick sample determined by CPM (squares) and from the ratio r_{CPM} (inverted triangles) with the spin density measured by electron spin resonance (ESR) (triangles). The CPM and the r_{CPM} data were scaled to match the spin density for long illumination times. The three sets of data follow the same time behavior characterized by a power-law time dependence of the type $N_s \sim t^{\eta}$, with $\eta=\frac{1}{3}$.

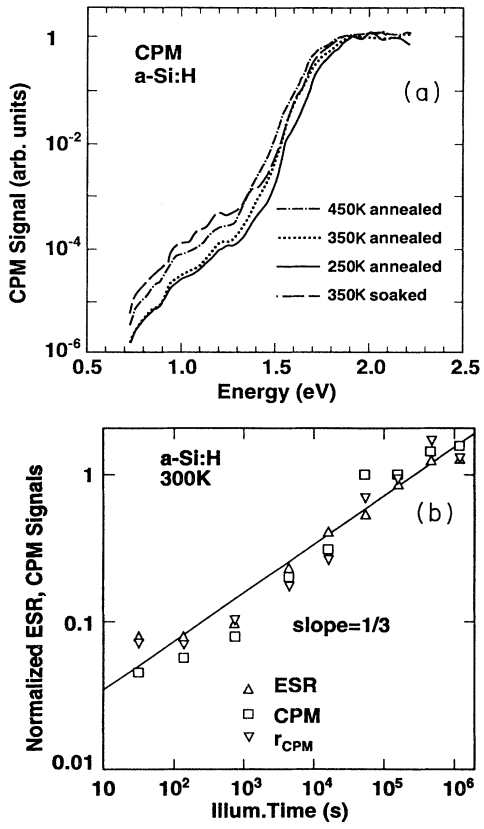

FIG. 1. (a) CPM spectra for an a-Si:H sample measured at different temperatures. The spectra are normalized to the same intensity at 2.0 eV. (b) Time evolution of the light-induced defect density in a 15-μm-thick a-Si:H sample, measured by ESR (triangles), CPM (squares), and the fast CPM procedure (r_{CPM}) described in the text (inverted triangles).

III. RESULTS

Figure 2 shows the time dependence of the light-induced defect density at different temperatures, for a fixed light flux of 2800 mW/cm^2. The time dependence of the defect creation process is shown here only to indicate that a steady state has been achieved and will be dealt with in a subsequent publication.[11] The initial defect density in each case was determined by CPM prior to illumination. Above room temperature the defect density saturates around $(5-10)\times 10^{16}$/cm^3 for the highest illumination intensity used. The saturation values decrease

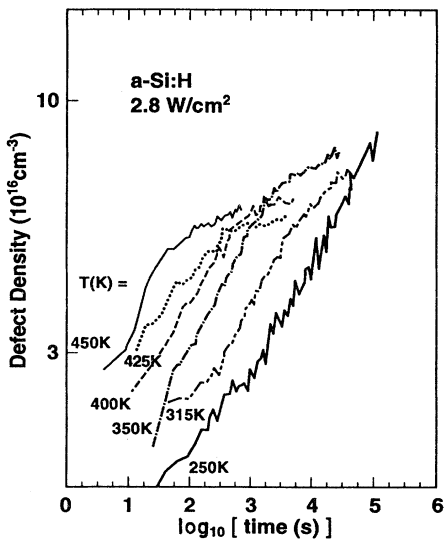

FIG. 2. Time evolution of the light-induced defect density in a-Si:H measured at different temperatures. The same was irradiated with 2.8 W/cm^2 of monochromatic light (1.92 eV) from a Kr^+ laser.

slightly with increasing temperatures. By observing the decay of the defect density after the light was shut off, we verified that the saturation is not due to partial annealing of light-induced defects when the illumination is interrupted to measure the defect density. At room temperature and below a clear saturation is not observed, even after $\sim 10^5$ s of strong illumination. The curves, however, display an inflexion point indicating reduced defect formation rates and the approach of saturation.

Figure 3 shows the temperature dependence of the defect density in the annealed state before soaking (dots) and in the saturated light-soaked state (open symbols). The defect density in the annealed state is constant below 390 K. Above this temperature, the defect density increases with an activation energy of 0.20–0.22 eV. We attribute the increase in the defect density to thermal equilibration of defects in the *a*-Si:H network.[12] For comparison, the solid triangles in the figure display the equilibrium spin density determined by ESR in *a*-Si:H films quenched to room temperature as a function of the quenching temperature T.[7] The spin density agrees well with the CPM defect density measured in our samples.

The open symbols in Fig. 3 correspond to the saturated defect density under different illumination intensities. The saturation density decreases with increasing temperature, and the effect is stronger for low illumination intensities. Where a clear saturation was not achieved, an arrow was added to the data point to indicate a lower limit for the saturation density. It is remarkable that the saturation density depends very weakly on the illumination intensity. An increase in the illumination intensity by a factor of ~ 30 at 400 K leads to only a doubling of the steady-state density. If a power-law dependence of the type $N_{s,\infty} \sim G^{\epsilon}$ is assumed, the exponent $\epsilon \sim 0.2$ at 400 K and decreases at lower temperatures. These results are in contrast with those reported recently by Park, Liu, and Wagner,[9] who reported a saturation density at room temperature independent of the light-induced carrier generation rate.

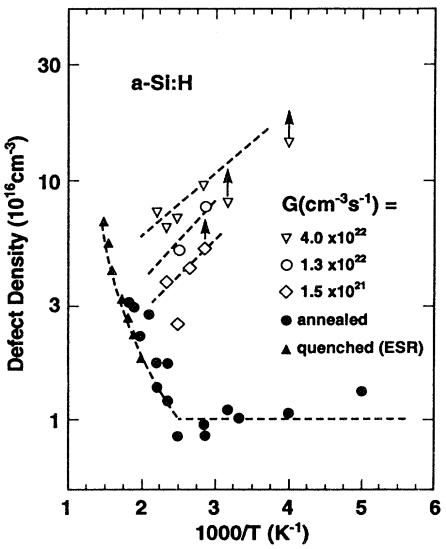

FIG. 3. Defect density in the annealed state before illumination (solid dots) and after irradiation with 2.8 W/cm^2 (inverted triangles, corresponding to a carrier generation rate of $G = 4.0 \times 10^{22}$ cm^{-3}s^{-1}), 0.70 W/cm^2 (open circles, $G = 2.5 \times 10^{22}$ cm^{-3}s^{-1}), and 0.065 W/cm^2 (diamonds, $G = 1.5 \times 10^{21}$ cm^{-3}s^{-1}). The dashed lines are guides for the eye. The solid triangles represent the ESR spin density measured at room temperature after quenching *a*-Si:H films from different temperatures (from Ref. 7).

IV. CHEMICAL MODEL FOR THE STEADY-STATE DENSITY OF LIGHT-INDUCED DEFECTS

The dependence of the saturation density $N_{s,\infty}$ on the illumination intensity and on temperature suggests that saturation is due not to depletion of precursor sites for defect formation, but rather to a balance between defect generation and annealing, such as required by the chemical equilibrium model. In the following, we will first review models for the equilibrium defect density in *a*-Si:H. These models will then be extended to include defect formation under illumination. In the last part of this section the predictions of the model will be compared with the experimental data presented above.

Recently, Winer and Street,[7,8] examined thermodynamic models for the equilibrium defect density in undoped *a*-Si:H based on a chemical equilibrium between weak Si—Si bonds (SiSi) and neutral dangling bonds (Si—) in the amorphous network. The defect density in the dark is well explained by a chemical equilibrium reaction expressed by[7]

$$\mathrm{SiH} + (\mathrm{SiSi}) + E_{\mathrm{thermal}} \rightleftharpoons (\mathrm{Si}—) + (\mathrm{SiHSi}—) \ . \qquad (1)$$

Chemical equilibration at low temperatures takes place through the motion of hydrogen atoms from bond terminating sites (SiH) to weak-bond sites (SiSi) that make the valence-band tail of localized states, leading to the formation of two defects: (i) an isolated dangling bond Si— in the original hydrogen site SiH and (ii) a complex consisting of a dangling bond adjacent to a SiH bond, which cannot be separated from each other. Both defects have the same density N_D so that the total defect density is $N_s = 2N_D$.

Quantitative prediction of the equilibrium defect density requires an estimate of the enthalpy change for the forward reactions in Eq. (1), corresponding to the formation energy $2U_{f0}$ of two neutral defects. In the framework of the weak-bond model, U_{f0} is the energy necessary to promote an electron from the initial weak-bond state in the valence-band tail (E_{VB}) to the defect state in the gap (E_D), i.e., $U_{f0}(E_{\mathrm{VB}}) = E_D - E_{\mathrm{VB}}$.[13] The energy reference is taken to be the valence-band mobility edge. In a more realistic model that will not be considered here, a distribution of defect energies E_D can be taken into account.[12] The weak bonds are assumed to have an exponential energy distribution given by $N_v(E_{\mathrm{VB}}) = N_{V0} \exp(-E_{\mathrm{VB}}/kT_v)$, where kT_v is the exponential slope of the valence-band tail.[6] The equilibrium density of weak bonds converted to defects N_D can be shown to be the solution of the following integral equation:[7,12]

$$N_D=\int_0^\infty \frac{N_v(E_{\rm VB})dE_{\rm VB}}{1+(N_D/N_H)\exp[2U_{f0}(E_{\rm VB})/kT]}$$
$$=\int_0^\infty \frac{N_v(E_{\rm VB})dE_{\rm VB}}{1+\exp[2(\mu_0-E_{\rm VB})/kT]}\ , \tag{2a}$$

where the integration is over the distribution of valence-band tails states and

$$\mu_0=U_{f0}(E_{\rm VB})+E_{\rm VB}+\frac{kT}{2}\ln\frac{N_D}{N_{\rm H}}=E_D+\frac{kT}{2}\ln\frac{N_D}{N_{\rm H}} \tag{2b}$$

is an effective defect chemical potential describing the equilibrium between defects and weak bonds. It is easy to see from Eq. (2a) that at a given temperature most of the weak bonds with energy above μ_0 are converted to defects. Equation 2(a) satisfactorily explains the temperature dependence of the equilibrium defect density in *a*-Si:H.[7]

In order to extend the chemical equilibrium model to estimate the steady-state defect density under illumination, we must include the effects of carrier on the equilibrium between the two sides in reaction (1). The presence of electrons and holes is assumed to increase the rate of defect formation according to the reaction

$$\text{SiH}+(\text{SiSi})+e+h\rightleftharpoons(\text{Si—})+(\text{SiHSi—})\ . \tag{3}$$

In the modified reaction the presence of photogenerated carriers shifts the equilibrium to the right side thereby giving rise to photogenerated defects. A quantitative estimate of the steady-state equilibrium of reaction (3) is obtained by assuming that the carrier populations equilibrate on a time scale much shorter than defect generation. The distributions of electrons and holes thermalize within the bands and are described by electron (E_{Fn}) and hole (E_{Fp}) quasi-Fermi levels, respectively. The net defect formation energy of reaction (3) is reduced by the energy gained by dropping an electron from E_{Fn} to the defect state and by raising a hole from E_{Fp} to E_D.

The total net enthalpy change $2U_f(E_{\rm VB})$ in reaction (3) for the conversion of a weak bond with electronic energy $E_{\rm VB}$ into two defects can be written as

$$2U_f(E_{\rm VB})=2(E_D-E_{\rm VB})-(E_{Fn}-E_D)-(E_D-E_{Fp})\ . \tag{4}$$

The equilibrium defect density under illumination, still given by Eq. (2), is obtained by substituting U_f from Eq. (4) for U_{f0}. The defect chemical potential μ under illumination becomes

$$\mu=\frac{1}{2}\left[2E_D-(E_{Fn}-E_{Fp})-kT\ln\frac{N_D}{N_{\rm H}}\right]\ . \tag{5}$$

μ depends on the quasi-Fermi levels and therefore on the generation rate G. With increasing illumination levels, μ moves closer to the valence-band edge, and more weak bonds are transformed into defects. The newly created recombination centers reduce the quasi-Fermi level separation $E_{Fn}-E_{Fp}$, inhibiting further defect formation.

In order to obtain the defect density using Eq. (5) it is necessary to relate the quasi-Fermi levels E_{Fn} and E_{Fp} to the defect density and to the carrier generation rates G. We will assume the following simple relation between G, N_s, and E_{Fn}:

$$n_f=N_c e^{-(E_c-E_{Fn})/kT}=\frac{G^{\gamma_n}}{A_n N_s^{\delta_n}}+N_c e^{-E_a/kT} \tag{6a}$$

with $\gamma_n\sim 1$, n_f is the free-electron density, and $0.6<\delta_n<1.2$.[14,15] Here, E_c is the mobility gap, $N_c=1.25\times10^{20}(T/300\ \text{K})^{3/2}\ \text{cm}^{-3}$ (Ref. 16) is the effective density of states at the mobility edge, E_a is the activation energy for the dark conductivity, and A_n is the effective electron capture probability of the recombination centers. The first term on the right-hand side is the photogenerated free carrier density and the second term is the density of thermally generated carriers. The corresponding relation between the free hole density p_f and E_{Fp} is

$$p_f=N_v e^{-E_{Fp}/kT}=\frac{G^{\gamma_p}}{A_p N_s^{\delta_p}}+N_c e^{-(E_c-E_a)/kT}\ . \tag{6b}$$

The saturation defect density $N_{s,\infty}$ under illumination follows from the self-consistent solution of Eqs. (2) and (5) using Eq. (6). A useful analytical approximation is obtained by noting that for temperatures low enough for the thermal generation rate to be negligible [factor containing the activation energy in Eq. (6)] the integrand in Eq. (2) is equal to $N_v(E_{\rm VB})$ for $E_{\rm VB}\gg\mu$, and to $N_v(E_{\rm VB})\exp[-2(\mu-E_{\rm VB})/kT]$ for $E_{\rm VB}<\mu$. This leads to the following analytical approximation for the saturation defect density N_s^∞:

$$N_s\approx 2\left[k\left[\frac{2T_v^2}{2T_v-T}\right]N_{v0}\right]^{2/\zeta}\exp\left[-\frac{2E_D-E_c}{\zeta kT_v}\right]\times\left[\frac{N_{\rm H}G^{(\gamma_n+\gamma_p)}}{4A_nN_cA_pN_v}\right]^{\beta/\zeta} \tag{7a}$$

with

$$\zeta=2+\beta(1+\delta_n+\delta_p) \tag{7b}$$

and the temperature dependence is included in the variable β defined by

$$\beta=T/T_v\ . \tag{7c}$$

Equation (7) predicts a power-law dependence of the saturation defect density on the general rage G with a temperature-dependent exponent $\epsilon=(\gamma_n+\gamma_p)\beta/[2+\beta(1+\delta_e+\delta_p)]$. Assuming that $T_v=550$ K, $\gamma_n=\gamma_p=1$, $\epsilon=0.27$, 0.30, and 0.35 at 250, 300, and 400 K, respectively, which approximately agrees with the experimental results.

In order to test the chemical equilibrium model described above more thoroughly, the steady-state defect density under illumination was calculated from Eqs. (2) and (5) [without using the suppositions that led to Eq. (7)]. The parameters used in the calculations, summarized in Table I, are similar to the ones used by Street and

TABLE I. Parameters used in the calculations.

Parameter	Description	Value[a]
E_G	Band gap	1.6 eV
E_D	Defect level	0.6 eV
T_v	VB temperature	550 K
U_C	Correlation energy	0.3 eV
N_{v0}	Density of VB tail states	2×10^{20} cm^{-3} eV^{-1}
$A_n^{\dagger b}$	Electron capture probability	3×10^{-9} cm^3/s
$A_p^{\dagger b}$	Hole capture probability	0.8×10^{-0} cm^3/s
N_H	Hydrogen density	5.0×10^{21} cm^{-3}

[a]Energy values measured with respect to the valence-band mobility edge.

[b]From Ref. 2. These capture probabilities were scaled to obtain the results in Fig. 3 (see discussion in text).

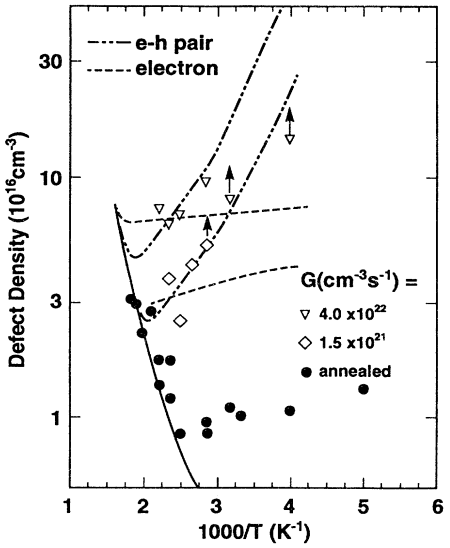

FIG. 4. Steady-state defect density under illumination for defect formation reaction involving an electron-hole pair (—··—··) and one electron (— — —). In each case, the upper and lower curves are for generation rates of 4.0×10^{22} and 1.5×10^{21} cm^{-3}s^{-1}, respectively. The solid line is the calculated defect density in the dark. The curves are superposed on the experimental data of Fig. 3.

Winer[7] to describe the temperature dependence of the equilibrium defect density in the dark. Other parameters necessary for the determination of the defect density under illumination like $\delta_{n,p}$ and $\gamma_{n,p}$ are not well known and may in fact depend on the defect density. We assumed $\delta_{n,p}=\gamma_{n,p}=1$ and $E_a=E_c-E_D$, i.e., the defect equilibrium Fermi level to coincide with the defect level E_D. In order to shift the curves vertically to superpose with the experimental data, the capture probabilities A_n and A_p were scaled by a factor of 1.5×10^3. Such large capture probabilities are unrealistic and probably arise from an overestimation of the carrier-induced reduction in formation energy. No scaling of A_p and A_n is necessary if either the quasi-Fermi level shifts are reduced by ~0.25 eV or the defect level E_D increased by the same amount. A more accurate relation between the photogenerated carrier concentration G and the defect density N_s is needed to resolve the absolute magnitude of the calculated values. The approximate expression given by Eq. (7) reproduces the more exact numerical results to within 10% below ~400 K.

The model is consistent with the observed intensity and temperature dependence of the steady-state defect density. In Fig. 4, the steady-state defect density from the model under illumination for two different intensities (dot-dashed lines) and in the annealed state (solid line) is superimposed on the experimental data of Fig. 3. Above 450 K the defect density increases as a function of temperature both under illumination and in the annealed state. This occurs because the thermally generated carrier density, which increases with temperature, dominates the optically induced carrier density. The defect density does not depend on light intensity and increases with an effective activation energy of 0.2–0.3 eV. There is essentially no light-induced defect formation above this temperature. This agrees well with the annealed CPM data (solid circles) as well as ESR data on rapidly quenched samples (triangles, Fig. 3).

Below 450 K the density of optically generated carriers dominates that of thermally generated carriers, which decreases with temperature. The model predicts the observed weak intensity dependence of the steady-state defect density rather well. A large increase in light intensity increases the electron and hole densities thereby increasing the defect generation rate. An increased defect density greatly reduced the electron and hole densities, suppressing defect generation. Furthermore, the number of potential defect sites increases exponentially with $E_{Fn}-E_{Fp}$. As a consequence of all these factors working against a defect density increase, even a large increase in light intensity does not greatly alter the defect density resulting in a weak dependence of the equilibrium defect density on light intensity. The dependence is so weak that at first it appears to be independent of intensity.

The model also does a fair job in accounting for the weak temperature dependence of the steady-state defect density. The steady-state defect density decreases with increasing temperature because the generation rate, proportional to the density of photogenerated electrons and holes, is temperature independent but the annealing rate increases with temperature. The temperature dependence can be easily understood by recalling that $N_{s,\infty}$ is determined by the steady-state quasi-Fermi levels E_{Fn}^{∞} and E_{Fp}^{∞}. In the low-temperature regime, the density of photogenerated carriers is much larger than that of thermally excited carriers and $E_{Fn}^{\infty}\approx E_C-kT\ln[A_nN_c(T)N_{s,\infty}/G]$, with a similar expression for E_{Fp}^{∞}. Neglecting the weak (logarithmic) dependence of E_{Fn}^{∞} and E_{Fp}^{∞} on $N_{s,\infty}$, it is easy to see that with increasing temperature the quasi-Fermi levels shift toward midgap, decreasing the saturation defect density. The effective activation energy for $N_{s,\infty}$ is small (0.1–0.15 eV). The agreement of the model with experiment below 450 K would even be better if a clear steady-state defect density could be obtained at low temperatures. The

points with the arrows indicate the higher obtained defect density and therefore represent lower limits for the steady-state values. The expected saturation values are 2–3 times larger.

Finally, we investigated other defect formation reactions involving one or two carriers. A reaction similar to Eq. (3) but involving just one electron (not discussed in detail here) gives rise to the dashed line in Fig. 4, which does not seem to be consistent with experiment. Reactions involving two electrons (or two holes) lead to results similar to those obtained for the electron-hole reaction displayed in Fig. 4, and can in principle not be discarded as a possible formation mechanism for light-induced defects. The important point is that these equilibration models involving the conversion of weak bonds into defects can account for both the weak temperature and light-intensity dependence of the steady-state density of light-induced defects.

V. CONCLUSIONS

We presented experimental data on the saturation value for the light-induced defect density over a wide range of illumination intensities and temperatures. The weak temperature and light-intensity dependence of the steady-state defect density can be accounted for by a chemical equilibrium model for the defect density under illumination, similar to the one used to account for the equilibrium defect density in the dark and carrier induced defect generation.[7] The increased defect density under illumination is due to a decrease in the effective defect formation energy, when the electron (or hole) quasi-Fermi energy is moved towards the conduction (valence) band. Defect generation under illumination is a self-limiting process and the defect density reaches a saturation value at long illumination time despite the existence of an extended distribution of weak bonds, which can be converted into defects.

ACKNOWLEDGMENTS

We thank Kris Winer and L. Ley for helpful discussions. The research was supported by the Solar Energy Research Institute (Golden, CO).

[1]D. L. Stabler and C. R. Wronski, Appl. Phys. Lett. **31**, 292 (1977).
[2]M. Stutzmann, W.B. Jackson, and C. C. Tsai, Phys. Rev. B **32**, 23 (1985).
[3]R. A. Street, M. Hack, and W. B. Jackson, Phys. Rev. B **37**, 4209 (1988).
[4]W. B. Jackson and J. Kakalios, in *Amorphous Silicon and Related Materials,* edited by Hellmut Fritzsche (World Scientific, Singapore, 1988), p. 247.
[5]R. A. Street, J. Kakalios, C. C. Tsai, and T. M. Hayes, Phys. Rev. B **35**, 1316 (1987).
[6]Z. E. Smith and S. Wagner, Phys. Rev. Lett. **59**, 688 (1987).
[7]R. A. Street and K. Winer, Phys. Rev. B **40**, 6236 (1989).
[8]K. Winer, Phys. Rev. B **41**, 12 150 (1990).
[9]H.R. Park, J. Z. Liu, and S. Wagner, Appl. Phys. Lett. **55**, 2658 (1989).
[10]D. Redfield, Appl. Phys. Lett. **48**, 846 (1986).
[11]P. V. Santos and W. B. Jackson (unpublished).
[12]K. Winer, Phys. Rev. Lett. **63**, 1487 (1989).
[13]M. Stutzmann, Philos. Mag. B **57**, 63 (1987).
[14]W. B. Jackson, Philos. Mag. Lett. **59**, 103 (1989).
[15]C. R. Wronski, Z. E. Smith, S. Aljishi, V. Chu, K. Shephard, D.-S. Shen, R. Schwartz, D. Slobodin, and S. Wagner, in *Stability of Amorphous Silicon Alloy Materials and Devices,* edited by B. L. Stafford and E. Sabisky, AIP Conf. Proc. No. 157 (AIP, New York, 1987), p. 172.
[16]N. Ashcroft and N. D. Mermin, *Solid State Physics* (Holt-Rinehardt and Winston, New York, 1976).